Determination of Effective Connectivity of Brain Activity in the Resting Brain

Catarina Pião Azevedo[1], Paulo A. Salgado[1], T.-P. Azevedo Perdicoúlis[1], and Paulo Lopes dos Santos[2(✉)]

[1] ECT, UTAD, Vila Real 5000-811, Portugal
{psal,tazevedo}@utad.pt
[2] FEUP, UP, Porto 4200-465, Portugal
pjsantos@fe.up.pt

Abstract. The resting brain has been extensively investigated for low frequency synchrony between brain regions, namely Functional Connectivity. However the other main stream of the brain connectivity analysis that seeks causal interactions between brain regions, Effective Connectivity, has been still little explored. Inherent complexity of brain activities in resting-state, as observed in Blood Oxygenation-Level Dependant fluctuations, calls for exploratory methods for characterizing these causal networks [1].

To determine the structure of the network that causes this dynamics, it is developed a method of identification based on least squares, which assumes knowledge of the signals of brain activity in different regions. As there is no access to functional Magnetic Resonance Imaging, data it is developed a model to obtain the Blood Oxygenation Level Dependent signals and it is implemented a reverse hemo-dynamic function. To assess the performance of the created model Monte Carlo simulations have been used.

Keywords: State-Space Model · Functional Magnetic Resonance Imaging · Monte Carlo Simulation · Effective Connectivity · Independent Component Analysis

1 Introduction

In resting-state functional Magnetic Resonance Imaging (fMRI), a non-invasive neuroimaging technique that uses strong magnetic fields and radio waves to measure changes in blood flow and oxygenation throughout the brain, researchers have observed low-frequency fluctuations of brain activity that are difficult

P. A. Salgado—Supported by FCT - Fundação para a Ciência e a Tecnologia under project UIDB/04033/2020.
T.-P. A. Perdicoúlis—Supported by FCT - Fundação para a Ciência e a Tecnologia under project IDB/00048/2020.
P. L. Santos—Supported by FCT - Fundação para a Ciência e a Tecnologia under project UIDB/50014/2020.

A. Cunha et al. (Eds.): MobiHealth 2023, LNICST 578, pp. 17–32, 2024.
https://doi.org/10.1007/978-3-031-60665-6_2

to explain. Raichle and colleagues proposed the concept of "dark energy" to describe this phenomenon, which refers to the energy associated with these mysterious fluctuations. Interestingly, when the brain transitions from rest to performing a task, the energy of these fluctuations does not increase significantly. By studying the resting brain, researchers hope to gain a better understanding of its intrinsic activity [2].

To unravel the enigma that is the brain's "dark energy", a wide variety of machine learning and signal processing methods and algorithms have been proposed [1]. These methods reveal a low frequency synchrony, Functional Connectivity (FC) [3], within specific networks of brain regions. This issue has been extensively studied, and there are efficient methods to determine these networks. One of these methods is the Independent Component Analysis (ICA) which is a computational technique used to separate a multivariate signal into independent non-Gaussian components. ICA can be used to decompose complex signals, such as those obtained from fMRI, into their underlying neural sources. This allows researchers to identify patterns of neural activity that are not readily apparent in the raw data and can aid in the investigation of brain function and connectivity [4].

However, the other main stream of research in brain connectivity analysis, Effective Connectivity (EC) [3], is the one that we are going to use in this study. Effective Connectivity is introduced to represent the causal influences that each region of the brain exerts over other regions. In fact, there are some aspects of on-going brain activity which cannot be described by inadequate measures of instantaneous coupling, so causal inferences should be employed for better understanding of the neuronal system. Particularly, the activation/deactivation dichotomy of brain areas which can be regularly observed in resting-state Blood Oxygenation-Level Dependant (BOLD) signals, which are a measure of changes in blood oxygenation resulting from neural activity in a brain region and are used to identify active brain regions during specific tasks or activities, should be revisited in a cause and effect view within brain dynamics and structure, rather than evolved patterns of synchrony in brain activity [5]. The low-frequency fluctuations of bold signals reveal a signal transmission dynamics that depends on the structure of the networks connecting different brain regions. The goal is to determine the structure of the network that causes this dynamics.

In this paper, we developed a method of identification based on least squares, which assumes knowledge of the signals of brain activity in different regions of the brain. As fMRI does not directly measure these signals, they are obtained through filters with impulse responses equal to inverse hemo-dynamic functions excited by the BOLD signals, i.e., the signals that are measured by fMRI. This methodology is illustrated in Fig. 1 and Fig. 2. The contributions of this work are: (i) A method of identification based on least squares, which assumes knowledge of the signals of brain activity in different regions, to determine the structure of the network that causes the dynamics. (ii) it is developed a model to obtain the Blood Oxygenation Level Dependent signals and it is implemented a reverse

hemo-dynamic function as there is no access to functional Magnetic Resonance Imaging data. (iii) Simulation of the brain activity at rest.

In Sect. 2, we describe the state-space models which are used throughout this paper. In Sect. 3, we demonstrate how the matrix structure can be determined when we have access to the signals from the brain network. As we do not have access to fMRI data, we develop, in Sect. 4, a simulation model that allows for obtaining the BOLD signals. The inverse hemo-dynamic functions to obtain the brain activity signals through BOLD signals are implemented in Sect. 5. In Sect. 6 we illustrate the performance of the developed method using Monte Carlo simulations. Finally, we close with some conclusions and pointing out some directions for future work.

2 State-Space Models

In light of the complexity of observed activity patterns in the resting brain, and in response to questions regarding their generative mechanisms, investigators have developed mathematical models of neuronal communication. Such models allow for inferring, relating, and predicting the dependence of measured communication dynamics on the topology of brain networks [12].

According to recent controversies on different Effective Connectivity detection algorithms in [11] state-space models are used in EC because they can separate the modelling of latent neuronal activity from the hemo-dynamic response function. Additionally, these models allow for a control theory interpretation of causality in connectivity analysis, providing insight into causal interactions in the brain system [1].

Communication models can be roughly classified into three types: dynamical, topological, and information theoretical. Dynamical models aim to capture biophysical mechanisms of signal transformation and transmission, while topological models propose network attributes to explain activity patterns. Information theoretical models use statistical measures to quantify interdependence, direction, and causality between nodes.

2.1 Dynamic Models and Measures

Dynamical models also differ in terms of the spatiotemporal scales of phenomena that they seek to explain. The choice of the explanatory scale impacts the precise communication dynamics that the model produces, as well as the scale of collective dynamics that can emerge. The general form of a deterministic dynamical model at an arbitrary scale is given by [13]

$$\frac{dx}{dt} = f(x, A, u, \beta). \tag{1}$$

Here, x encodes the state variables that are used to describe the state of the network, A encodes the underlying connectivity matrix, and u encodes the input variables. The functional form of f is set by the requirements (i.e., the expected

utility) of the model. Finally, β encodes other parameters of the model, independent of the connectivity strength A. The β parameters can be phenomenological, thereby allowing for an exploration of the whole phase space of possible behaviours; alternatively, the β parameters can be determined from experiments in more data-driven models [13].

The use of temporal precedence and lead-lag relationships is also a basis for alternative definitions of causality. Notably, this relationship can be used to measure the causal effect between neural masses coupled according to the structural connectome [14].

2.2 Topological Models and Measures

It has been believed that long routes in a network are metabolically costly and result in slower signal propagation [18]. Therefore, shortest paths are often used to infer the efficiency of communication between two regions. However, relying solely on shortest paths has been questioned for three reasons. First, networks that depend solely on shortest paths are vulnerable to targeted attacks. Second, investing solely in shortest paths means that alternative routes are underutilized and this is not optimal. Third, routing a signal by the shortest path would require biologically implausible knowledge of the global network structure [15].

By denoting the adjacency matrix by A, we can define the communicability between node i and node j as the weighted sum of all walks starting at node i and ending at node j [16]

$$G_{ji} = \sum_{k=0}^{\infty} c_k (A^k)_{ji}, \tag{2}$$

where A^k denotes the k-th power of matrix A, and c_k are the coefficients chosen to ensure convergence of the series and to give less weight to longer paths. If all entries of A are non-negative (which is often the case in communicability), the resulting values of G_{ji} are also non-negative and real.

2.3 Information Theoretic Models and Measures

Information theory and statistical mechanics have been used to develop measures of information transfer in brain networks such as transfer entropy and Granger causality [19]. These measures rely on the fact that the propagation of signals through the brain networks generates time-dependent activity patterns that can be measured as time series. Entropic measures of communication aim to identify statistical relationships between these time series, in order to infer the amount and direction of information transfer between different brain regions.

A central concept in information theory is the Shannon entropy [17], which quantifies the uncertainty in a discrete random variable I that follows the probability distribution $p(i)$. It is defined as $H(I) = -\sum_i p(i) log(p(i))$. Another measure of statistical interdependence between two random variables I and J

is their mutual information, $M_{IJ} = \sum p(i,j) \frac{log(p(i,j))}{log(p(i)), log(p(j))}$, where $p(i,j)$ is their joint distribution and $p(i)$ and $p(j)$ are their marginal distributions. However, since mutual information is symmetric, it does not capture the direction of information flow between two processes or sequences of random variables [17].

Transfer entropy takes into account the transition probability between different states, which can be the result of a stochastic dynamic process and obtained from the time series of activities of brain regions through imaging techniques. To measure the direction of information transfer between processes I and J, the notion of mutual information is generalized to the mutual information rate. The transfer entropy between processes I and J is given by [17]

$$T_{J \to I} = \sum p(i_{n+1}, i_n^k, j_n^l) log \frac{p(i_{n+1}|i_n^k, j_n^l)}{p(i_{n+1}|i_n^k)} \tag{3}$$

The processes I and J are assumed to be stationary Markov processes of order k and l, respectively. The quantity i_n^k, j_n^l denotes the state of process $I(J)$ at time n, while $p(i_{n+1}|i_n^k)$ denotes the transition probability to state i_{n+1} at time $n+1$, given knowledge of the previous k states. Similarly, $p(j_{n+1}|j_n^l)$ is the transition probability for process J. The quantity $p(i_{n+1}|i_n^k, j_n^l)$ is the same as $p(i_{n+1}|i_n^k)$ if the process J does not influence the process I.

3 Identification of Networks in the Resting Brain

It is important to notice that in this procedure, it is assumed that the hemodynamic response functions of different regions in the brain are known. These functions describe how neural activity in a particular brain region is converted into changes in blood flow and oxygenation, which are measured by fMRI signals. The hemo-dynamic response functions are used to model the relationship between brain activity and fMRI signals, and thus estimate the matrix A that relates brain activity to observed fMRI signals. It is important to have a good understanding of the hemo-dynamic response functions in order to properly model brain activity and obtain accurate estimates of matrix A.

According to [1], the brain activity measurement system at rest using functional magnetic resonance imaging (fMRI) can be described by the following linear time-invariant (LTI) state model:

$$z(t+1) = A_0 z(t) + q_0(t) \tag{4}$$

$$x_m(t) = \begin{bmatrix} z_m \\ z_m(t-1) \\ z_m(t-L+1) \end{bmatrix} \tag{5}$$

$$y_m(t) = c_m x_m(t) + r_m(t), m = 1, ..., M \tag{6}$$

The signals $y_m(t)$ represent the BOLD signals in the m brain regions that are measured by fMRI, while $q_0(t)$ and $r_m(t)$ are noise signals ($q_0(t)$ is process noise

and $r_m(t)$ is measurement noise, both of which are assumed to be Gaussian white noise). The goal is to estimate the matrix A_0 that defines the causal network structure of the resting brain based on the measurements of $y_m(t)$, $m = 1, \ldots, M$.

The row vectors c_m are formed by samples of hemo-dynamic response functions $h(t)$. It is important to note that, according to Eq. (4), each signal $y_m(t)$ is the convolution of $z_m(t)$ with a hemo-dynamic response function $h_m(t)$. This means that, as illustrated in Fig. 1, each signal $y_m(t)$ can be viewed as the output of a linear time-invariant (LTI) system excited by the signal $z_m(t)$. In Eqs. (4)–(6), it is assumed that these systems have finite impulse responses (FIR systems), i.e., that $c_m(t) = h_m(t)$ for $t = 0, \ldots, L$ and $c_m(t) = 0$ for $t > L$. However, existing studies on hemo-dynamic response functions conclude that these are impulse responses of LTI systems with infinite impulse responses, with orders significantly smaller than those of the FIR approximations [7]. Therefore, assuming FIR systems unreasonably increases the dimension of the model. Since the resting brain model is described by a state-space model, it makes sense to describe the convolution of the state variables with hemo-dynamic response functions as state-space models as well. This implies that the brain activity measurement system represented in Fig. 1 can be described by a state-space model of lower order than the model in Eqs. (4)–(6) assumed in [1]. In this context, $y_m(t)$ and $z_m(t)$, $m = 1, \ldots, M$, are related by state-space models of order n_m with $n_m << L$:

$$w_m(t+1) = A_m w_m(t) + B_m z_m(t) + q_m(t) \tag{7}$$

$$y_m(t) = C_m w_m(t) + D_m z_m(t) + r_m(t) \tag{8}$$

With $w_m(t) \in \mathbb{R}^{n_m}$, $A_m \in \mathbb{R}^{n_m \times n_m}$, $B_m \in \mathbb{R}^{n_m}$, $C_m \in \mathbb{R}^{1 \times n_m}$, and $D_m \in \mathbb{R}$ for $m = 1, \ldots, M$, combining Eqs. (4), (7), and (8) yields the following state-space model:

$$x(t+1) = A_x(t) + q(t) \tag{9}$$

$$y(t) = C_x(t) + r(t) \tag{10}$$

where

$$x(t) = \begin{bmatrix} z(t) \\ w_1(t) \\ w_2(t) \\ \vdots \\ w_M(t) \end{bmatrix} \tag{11}$$

$$y(t) = \begin{bmatrix} y_1(t) \\ y_2(t) \\ \vdots \\ w_M(t) \end{bmatrix} \tag{12}$$

$$A_x = \begin{bmatrix} a_1 & \cdots & a_M & 0_{M\times n_1} & \cdots & 0_{M\times n_M} \\ B_1 & \cdots & 0_{n_1} & A_1 & \cdots & 0_{n_1\times n_M} \\ 0_{n_2} & \cdots & 0_{n_2} & 0_{n_2\times n_1} & \cdots & 0_{n_2\times n_M} \\ \vdots & \ddots & \vdots & \vdots & \ddots & \vdots \\ 0_{n_M} & \cdots & B_M & 0_{n_M\times n_1} & \cdots & A_M \end{bmatrix} \tag{13}$$

$$C_x = \begin{bmatrix} D_1 & 0 & \cdots & C_1 & \cdots & 0_{1\times n_M} \\ 0 & D_2 & \cdots & 0_{1\times n_1} & \cdots & 0_{1\times n_M} \\ \vdots & \vdots & \ddots & \vdots & \ddots & \vdots \\ 0 & 0 & \cdots & 0_{1\times n_1} & \cdots & C_M \end{bmatrix} \tag{14}$$

$a_i \in \mathbb{R}^M, i = 1, \ldots, M$ are the columns of $A_0 \in \mathbb{R}^{M\times M}$, $x(t) \in \mathbb{R}^{n_x}, y(t) \in \mathbb{R}^M, A_m \in \mathbb{R}^{n_m\times n_m}, B_m \in \mathbb{R}^{n_m}, C_m \in \mathbb{R}^{1\times n_m}, D_m \in \mathbb{R}, m = 1, \ldots, M$, where $A \in \mathbb{R}^{n_x\times n_x}$ and $C \in \mathbb{R}^{M\times n_x}$, with $n_x = M + n_1 + \cdots + n_M$. If the system (9)–(10) is observable, then it can be identified by any algorithm that estimates models in state space; The problem is that these methods produce data-driven models, i.e., realizations determined by the data, different from those we intend to estimate and that are described by equations (9)–(14). Despite the orders of the models that relate $y_m(t)$ with $z_m(t)$ having been significantly reduced, the number of parameters remains very large.

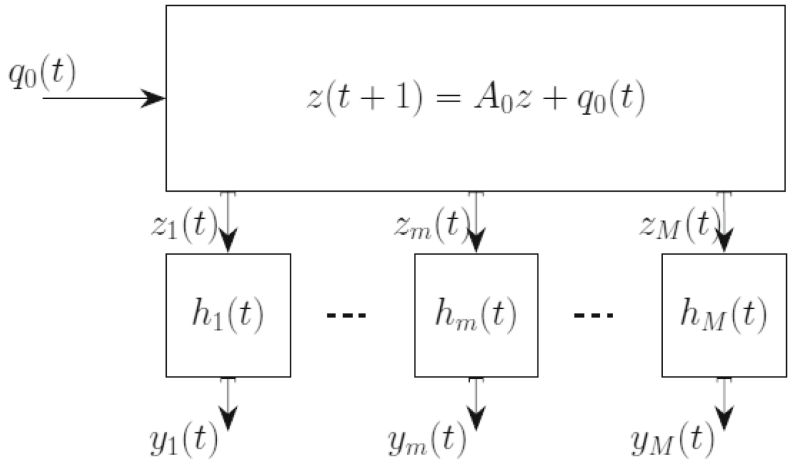

Fig. 1. The brain activity measurement system at rest using fMRI

4 Simulation Model of Resting Brain Activity and Functional Magnetic Resonance

4.1 Resting Brain Model

According to [1], the activity of a resting brain can be described by the state model:

$$z[k+1] = A_0 z[k] + q_0[k] \tag{15}$$

where $z(t) = [z_1(t), \ldots, z_M(t)]^T \in \mathbb{R}^M$, $q_0(t) \in \mathbb{R}^M$, and $A_0 \in \mathbb{R}^{M \times M}$. The components $z_m(t)$, $m = 1, \ldots, L$ are signals in different regions of the brain resulting from this activity, and the components of $q_0(t)$ are stimuli for brain activity. This is a sampled model of the continuous-time model:

$$\dot{z}(t) = A_c z(t) + q_c(t) \tag{16}$$

which models an underlying continuous system. The model (15) represents (16) at sampling instants. That is,

$$z[k] = z(kT_s) \tag{17}$$

where T_s is the sampling period. The relationship between (15) and (16) is well known and is given by the following equations:

$$A_0 = e^{AcT_s} \Leftrightarrow Ac = \frac{1}{T_s} \ln(A_0) \tag{18}$$

$$q_0[k] = \int_{kT_s}^{(k+1)T_s} e^{A(t-\tau)} q_c(\tau) d\tau. \tag{19}$$

The state $z(t)$ is indirectly measured through functional magnetic resonance imaging (fMRI), which acquires a vector of signals $y(t)$ of the same dimension as $z(t)$.

The components $y_m(t)$, $m = 1, \ldots, M$ of $y(t)$ are designated by BOLD and are the outputs of M linear time-invariant systems whose impulse responses are the hemo-dynamic response functions. Each system is excited by one and only one component $z_m(t)$ of $z(t)$ and has an output $y_m(t)$ that indirectly measures the brain activity in the m region of the brain. The continuous system is represented in Fig. 1. In this work, we consider that the hemo-dynamic response functions are equal to the canonical function [7,8] given by:

$$h_c(t) = K \left(\frac{t^5 e^{-t}}{5!} - \frac{1}{6} \frac{t^{15} e^{-t}}{15!} \right). \tag{20}$$

After applying the Laplace Transform, we obtain the transfer function

$$H_c(s) = K \frac{6(s+1)^{10} - 1}{6(s+1)^{16}}. \tag{21}$$

The objective of the simulation is to obtain

$$y[k] = \begin{bmatrix} y_1[k] \\ \vdots \\ y_M[k] \end{bmatrix}, \quad k = 1, \ldots, N, \tag{22}$$

that is, $y(kT_s)$ for $k = 1, \ldots, N$. Since the output signal is discrete-time with sampling period T_s, one might think that to perform the simulation it would be sufficient to generate a realization of white noise for the input $q_0[k]$, simulate the continuous-time system (15), discretize the transfer functions $H_m(s)$, $m = 1, \ldots, M$, and simulate the discrete-time systems, taking the signals $z_m[k]$ as inputs. However, for this procedure to be possible, it is necessary to postulate the evolution of the signals $z_m(t)$ between the sampling instants. Existing sampling methods typically assume that in these time intervals, the signals remain constant (ZOH) or are piecewise linear. These assumptions are not suitable for this problem since the components of $q_c(t)$ are not persistent signals.

4.2 Brain Activity Stimuli

Brain activity stimuli can be seen as sequences of impulses with random amplitudes that occur at random instants. To simulate these stimuli, we divide the sampling intervals into N_s parts and consider that the probability of an impulse with random amplitude and duration T_s/N_s occurring in each sub-interval is p. That is, the presence of an impulse in each of these sub-intervals follows a Bernoulli distribution. The number of impulses in each sampling interval follows a binomial distribution. Therefore, the average number of impulses in each sampling interval is given by

$$N_i = pN_s. \tag{23}$$

If we fix N_i (the average number of impulses in each sampling interval), we can calculate p through

$$p = \frac{N_i}{N_s}. \tag{24}$$

Given T_s, the sampling period, N_s, the number of divisions of each sampling interval, and p, the probability of an impulse occurring in each sub-interval, the probability of an impulse existing at each instant kT_s/N_s is then given by

$$q_c(t) = B \times U, \tag{25}$$

where B is a random variable with Bernoulli distribution $B(p)$ and U is a random variable with Gaussian distribution $N(0, \sigma^2)$.

5 Inverse Hemo-Dynamic Models

The identification of the system (9)–(14) by a subspace state identification method presents the following problems:

1. It is a stochastic identification problem and the estimated model can be non-minimum phase.
2. It is a high-order model with a large number of parameters.
3. The estimated realization is determined by the data and needs to be converted to that of the model (9)–(14).

These three coupled problems make it very difficult to obtain estimates of A_0 with acceptable precision unless some *a priori* knowledge about the hemo-dynamic response function is used. However, this can be estimated using fMRI [6]. Therefore, it makes sense for this work to consider that the different hemo-dynamic response functions $h_m(t)$ are known. Many studies consider this function to be equal to a canonical function [7,8] given by Eq. (20).

The function $h_c(t)/K$ is the impulse response of the LTI system with transfer function:

$$H_c(s) = K\frac{6(s+1)^{10}-1}{6(s+1)^{16}}. \tag{26}$$

In this work, we consider $h_m(t) = h_c(t)$, where $h_c(t)$ is the impulse response of the discretization $H_c(s)$ with $K_m = K$ randomly generated. That is, $y_m(t)$ is the output of a system with transfer function $K_m H_c(z)$ excited by $z_m(t)$, where $H_c(z)$ is the discretization of $H_c(s)$. The state variables $z_m(t)$, $m = 1, \ldots, M$, can be reconstructed, $\hat{z}_m(t)$, from $y_m(t)$ through simulation of the inverse systems of $K_m H_c(z)$, denoted by $H_m^i(z)$. Once $\hat{z}(t)$, $t = 1, \ldots, N$, is known, A_0 can be also estimated through

$$\hat{A}_0 = \hat{Z}_2^{\dagger}\hat{Z}_1, \tag{27}$$

where

$$\hat{Z}_1 = \left(\hat{z}(1)\cdots\hat{z}(N-1)\right), \tag{28}$$

$$\hat{Z}_2 = \left(\hat{z}(2)\cdots\hat{z}(N)\right), \tag{29}$$

The main difficulty of this approach lies in the computation of the inverse model because, on one hand, the transfer function is not proper and, on the other hand, although $H_c(s)$ is an inversely stable transfer function, the same does not hold for its corresponding continuous-time transfer function, $H_c(z)$.

The whole procedure is illustrated in Fig. 2.

Due to the large difference between the degrees of the numerator and denominator of the transfer function $H_c(s)$, it is convenient to determine the system in discrete time. The difference between the degrees of the numerator and denominator of the discrete transfer function $H_c(z)$ is one unit. Since we can only invert proper and strictly proper transfer functions (where the degree of the

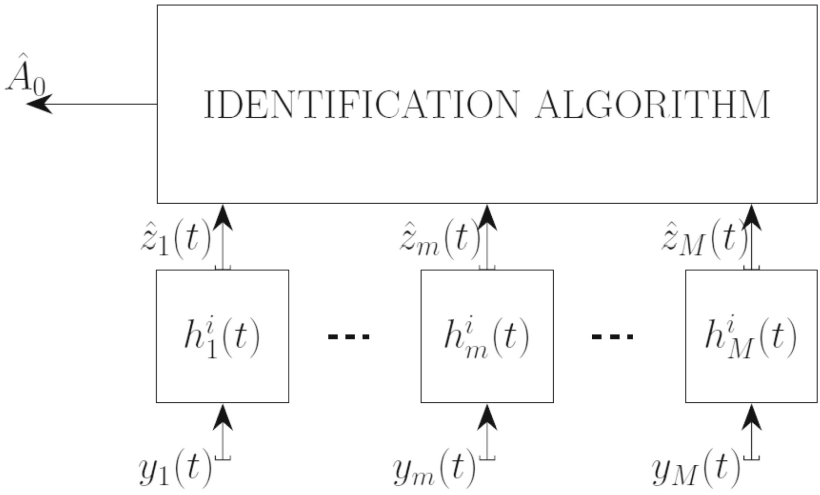

Fig. 2. The brain activity excitation signals are obtained from measurements at rest using the inverse fMRI signals

denominator is greater than or equal to the degree of the numerator), we need to multiply $H_c(z)$ by z before determining the inverse model. Multiplying $H_c(z)$ by z is equivalent to advancing the system output by one sampling period, so when we calculate $z_m(t)$ using the inverse model, this signal will be delayed by one sampling period. As mentioned earlier, there is still another difficulty, which is that the discrete versions of $H_c(s)$ are not inversely stable. Since the outputs $y_m(t)$ are stationary stochastic processes, we can maintain their spectral density by reflecting the unstable zeros of $H_c(z)$ inside the unit circle with a gain adjustment. Therefore, if we have

$$H_c(z) = (z - z_i)H_{cr}(z) \tag{30}$$

with $|z_i| > 1$, then

$$H_c^{min}(z) = \frac{(z - 1/\bar{z}_i)(1 - z_i)}{1 - 1/\bar{z}_i} H_{cr}(z) \tag{31}$$

where $\bar{z}_i$ is the complex conjugate of z_i, has frequency response with the same magnitude

$$|H_c^{min}(e^{jw})| = |H_c(e^{jw})|. \tag{32}$$

If two systems with transfer functions $H_c(z)$ and $H^{min}(z)$ are excited by the same stochastic process, then their outputs, although different, have the same spectral density. Therefore, by reflecting the unstable zeros of $H_c(z)$ inside the unit circle, we do not alter the spectral density of the signals $y_m(t)$, $m = 1, \ldots, M$.

6 Ilustration of the Performance of the Developed Method Through a Monte Carlo Simulation

Monte Carlo simulation is a computational technique used to estimate the probability of different outcomes in a system that is subject to random variables. It is named after the famous casino town of Monte Carlo, which is known for its games of chance. In a Monte Carlo simulation, a large number of random samples are generated from the distribution of each input variable. These samples are then used to simulate the system and calculate the probability of different outcomes. One of the key advantages of Monte Carlo simulation is its ability to incorporate uncertainty and variability into the analysis. By generating random samples from the input distributions, Monte Carlo simulation can provide estimates of the range of possible outcomes and their likelihoods, even when the input parameters are not precisely known [9,10].

We developed a Monte Carlo simulation that starts by defining several variables, including the true matrix of connections between brain areas (A_0), the sampling rate (T_s), the number of samples in the fMRI signal (N_s), the interval between samples in the fMRI signal (N_i), the number of brain areas (M), the number of points in the simulated brain activity signal (N), the number of Monte Carlo runs (N_{mc}), the noise standard deviation (σ), and the vector of the gains of the hemo-dynamic responses of each brain area (H).

Next, the simulation initializes a matrix to store the Monte Carlo results ($\hat{A}_{2,mc}$) and enters a Monte Carlo simulation loop. Within the loop, the code generates a simulated brain activity signal called q_c, simulates the fMRI signal called y, and estimates matrix A using the $\hat{Z}_{e_{mc}}$ matrix. The estimated matrix is then stored in the $\hat{A}_{2,mc}$ tensor. The equation for estimating A is given by

$$\hat{A} = \hat{Z}_{e_{mc}}(:, 2 : end)/\hat{Z}_{e_{mc}}(:, 1 : end - 1), \tag{33}$$

where $Z_{e_{mc}}$ is an $M \times N$ matrix representing the simulated fMRI signals for each brain area in each Monte Carlo run. The $\hat{A}$ matrix is an estimate of the state matrix A, which represents the dynamics of connections between brain areas.

The simulation creates histograms for each element of the estimated A matrix, calculates the standard deviation of each element of the estimated A matrix, and the mean and standard deviation of the estimated A matrices.

In a histogram, the variability of different parameters is represented by the distribution of values along the histogram bars. Each bar represents a range of values, and the height of the bar indicates the frequency or count of occurrences within that range.

When creating a histogram, we can observe the variability of different parameters through the dispersion or spread of values along the bars. If a parameter has lower variability, the values will be more concentrated around a central value, and the corresponding bars will be taller. On the other hand, if a parameter has higher variability, the values will be more dispersed, and the corresponding bars will be shorter, indicating a lower frequency in each range.

The following parameters were used:

$$A_0 = \begin{bmatrix} 0.7 & 0.31 & 0 & 0 & -0.46 \\ 0 & 0.7 & 0 & 0 & 0 \\ 0 & 0 & 0.7 & 0.55 & 0 \\ -0.38 & 0 & 0 & 0.7 & 0 \\ 0 & 0 & 0 & 0 & 0.7 \end{bmatrix}, \tag{34}$$

$$T_s = 1, \tag{35}$$

$$N_s = 10, \tag{36}$$

$$N_i = 1, \tag{37}$$

$$N = 1000, \tag{38}$$

$$N_{mc} = 100, \tag{39}$$

$$\sigma = 0.1, \tag{40}$$

$$H^T = \begin{bmatrix} 1.9005 & 0.9101 & 1.8404 & 1.3685 & 0.9977 \end{bmatrix}. \tag{41}$$

The equations involved in these calculations are

$$\sigma_{ij} = \mathrm{std}(\hat{A}_{ij}), \tag{42}$$

where σ_{ij} is the standard deviation of the (i, j) element of the estimated A matrix and $\hat{A}_{ij}$ is the (i, j) element of the estimated A matrix.

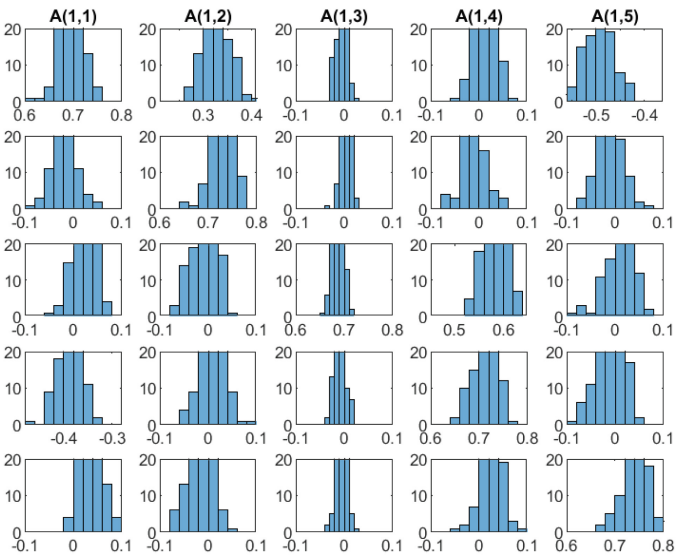

Fig. 3. Visualization of the distribution of the estimated values for each element of matrix A and comparison with the true value

$$\bar{A} = \text{mean}(\hat{A}_{mc}), \tag{43}$$

where $\bar{A}$ is the mean of the estimated A matrices and $\hat{A}_{mc}$ is the estimated A matrix for each Monte Carlo run. Also

$$\sigma_A = \text{std}(\hat{A}_{mc}) \tag{44}$$

where σ_A is the standard deviation of the estimated A matrices and $\hat{A}_{mc}$ is the estimated A matrix for each Monte Carlo run.

These equations are used to evaluate the reliability and stability of the A matrix estimation, as well as to evaluate the influence of different parameters on the estimation accuracy. They also help to understand the uncertainty in the A matrix estimation and provide useful information for the analysis of brain connections in fMRI signals.

Finally, the simulation displays the results and the mean value of the state matrix in a color scale, represented in Fig. 4.

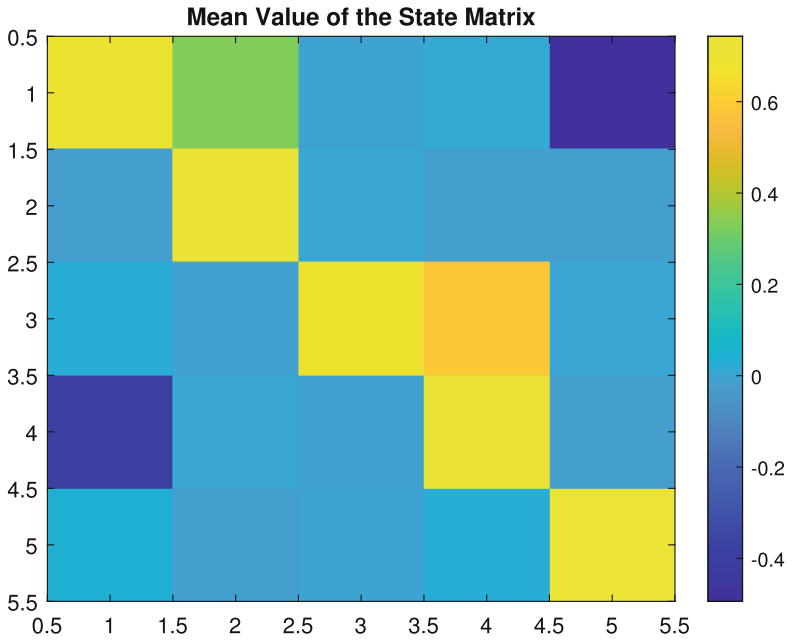

Fig. 4. Display of the results and the mean value of the state matrix in a color scale

Color scales are used to assign colors to data values in visualizations such as plots, images, and surfaces. When using a colormap, we can observe the variation in variability among different parameters through the intensity or hue of the colors assigned to them. Generally, darker colors represent lower values or lower

variability, while lighter colors represent higher values or greater variability. In this color scale, the colors range from dark blue to yellow, with light blue and green in between. The colors are assigned to a range of values in a dataset, with dark blue being the lowest value and yellow being the highest. More specifically, the color scale assigns the color dark blue to the minimum value in the dataset, and transitions through shades of light blue and green as values increase, before transitioning to shades of orange and yellow for the maximum value. The exact mapping of colors to values is nonlinear, which means that the perceived change in color is not constant as the values increase.

The performance of a Monte Carlo simulation depends on several factors, including the number of simulations, the complexity of the system being modelled, and the efficiency of the simulation algorithm. In general, increasing the number of Monte Carlo runs can improve the accuracy and reliability of the simulation results. Nonetheless we can state, through the analysis of Figs. 2 and 3, that the performance of our simulation is satisfactory because despite displaying variations in the average value of the state matrix they are not very significant (as most of the color scale is the same tone of blue, which corresponds to the same value).

7 Conclusions and Future Works

The determination of effective connectivity of brain activity in the resting state is a complex process that requires the use of sophisticated mathematical models and simulations. State-space models and inverse hemo-dynamic models have proven to be powerful tools for analyzing resting state fMRI data, allowing for the identification of key brain regions and their effective connections. The use of Monte Carlo simulations has further demonstrated the accuracy and reliability of these methods. Hence, through the development of a simulation model of resting brain activity and fMRI, we have been able to evaluate the performance of these methods and gain important insights into the functional organization of the brain. The findings have significant implications for understanding the neural mechanisms underlying brain function and for developing new diagnostic and therapeutic approaches for neurological and psychiatric disorders. Overall, the determination of effective connectivity of brain activity in the resting state holds great promise for advancing our understanding of the brain and improving human health.

One potential avenue for future research is the investigation of other mathematical models, such as deep learning algorithms, that may provide a more comprehensive understanding of the brain's functional organization. Additionally, the integration of multiple imaging modalities, such as fMRI, EEG, and MEG, could provide a more complete picture of the brain's effective connectivity. Also, a comparison with other methods available in the literature needs to be undertaken.

Acknowledgments. We would like to express our gratitude to the reviewers whose valuable suggestions greatly helped to improve this manuscript.

References

1. Bakhtiari, S.K., Hossein-Zadeh, G.A.: Subspace-based identification algorithm for characterizing causal networks in resting brain. NeuroImage **60**(2), 1236–1249 (2012). ISSN: 1053–8119. https://doi.org/10.1016/j.neuroimage.2011.12.075
2. Zhang, D., Raichle, M.E.: Disease and the brain's dark energy. Nat. Rev. Neurol. **6**, 15–28 (2010). https://doi.org/10.1038/nrneurol.2009.198. PMID: 20057496
3. Friston, K.J.: Functional and effective connectivity in neuroimaging: a synthesis. Hum. Brain Mapp. **2**, 56–78 (1994)
4. Tharwat, A.: Independent component analysis: an introduction. Appl. Comput. Inform. **17**(2), 222–249 (2018). https://doi.org/10.1016/j.aci.2018.08.006
5. He, B.J., Raichle, M.E.: The fMRI signal, slow cortical potential and consciousness. Trends Cogn. Sci. **13**, 302–390 (2009)
6. Friston, K.J.: Bayesian estimation of Dynamical systems: an application to fMRI. Neuroimage **16**, 513–30 (2002)
7. MLindquist, M.A., Loh, J.M., Atlas, L.Y., Wager, T.D.: Modeling the hemodynamic response function in fMRI: efficiency, bias and mis-modeling. NeuroImage **45**, S187–S198 (2009)
8. Henson, R., Friston, K.J.: Convolution models for fMRI. Statistical parametric mapping: the analysis of function brain images, pp. 178–192 (2007)
9. Muralidhar, K.: Encyclopedia of Information Systems. 1a edição. Academic Press, Cambridge (2002)
10. Harrison, R.L.: Introduction to Monte Carlo simulation. In: AIP Conference Proceedings, vol. 1204, pp. 17–21 (2010)
11. Friston, K.J.: Dynamic causal modeling and Granger causality Comments on: the identification of interacting networks in the brain using fMRI: model selection, causality and deconvolution. Neuroimage **58**, 303–305 (2011)
12. Srivastava, P., et al.: Models of communication and control for brain networks: distinctions, convergence, and future outlook. Netw. Neurosci. **4**, 1122–1159 (2020)
13. Breakspear, M.: Dynamic models of large-scale brain activity. Nat. Neurosci. **20** (2017)
14. Stam, C.J., van Straaten, E.C.W.: Go with the flow: use of a directed phase lag index (DPLI) to characterize patterns of phase relations in a large-scale model of brain dynamics. Neuroimage **62**, 1415–1428 (2012)
15. Avena-Koenigsberger, A., Misic, B., Sporns, O.: The physics of communicability in complex networks. Nat. Rev. Neurosci. **19**, 17–33 (2018)
16. Estrada, E., Hatano, N., Benzi, M.: Communication dynamics in complex brain networks. Phys. Rep. **514**, 89–119 (2012)
17. Schreiber, T.: Measuring information transfer. Phys. Rev. Lett. **85**, 461 (2000)
18. Bullmore, E., Sporns, O.: The economy of brain network organization. Nat. Rev. Neurosci. **13**, 336–349 (2012)
19. Valdes-Sosa, P.A., Roebroeck, A., Daunizeau, J., Friston, K.: Effective connectivity: influence, causality and biophysical modelling. Neuroimage **58**, 339–361 (2011)